Misan Journal of Engineering Sciences ISSN: 2957-4250
Vol. 4, No. 1, June 2025 ISSN-E: 2957-4242

Review for High Frequency Propagation Wave Through the Ionosphere Based on IRI Model Using Ray-Tracing Technique

Fatima Hikmat Ali[1*], Hasanain A. H. Al-Behadili[2], Nsaif Jasim Hadi[3] and A.J. Stocker [4]

[1]Department of Electrical Engineering, College of Engineering, University of Misan, *Maysan*, Iraq.
[2]Department of Ccommunication Engineering, College of Engineering, University of Misan, *Maysan*, Iraq.
[3]Department of Chemical Engineering, College of Engineering, University of Misan, *Maysan*, Iraq.
[4]Department of Ccommunication Engineering, College of Engineering, University of Leicester.
**Corresponding author E-mail:* enghs2307@uomisan.edu.iq

(Received 12 Jan, Revised 1 May, Accepted 4 May)

Abstract: The ionosphere's condition affects how HF radio waves propagate, which changes over time of day, season, and Solar activity conditions. These waves, when propagating through ions, are affected by several factors, including refraction, reflection, and absorption. To reduce these effects, ray tracing is an important tool that depends on atmospheric communication, relying on the IRI model to describe the ionosphere's parameters. This paper is an overview of the ionosphere and reviews the IRI model and ray tracing technique. IRI is acknowledged as the ionosphere's official standard by the organization for international standards, International Radio Science Union, Europe's collaboration with the Space Research Committee to promote space. According to these organizations, the IRI is a pilot (data-based) model that represents the basic parameters of the ionosphere based on the ion cover data record.

Keywords: Ionosphere, HF propagation wave, IRI, Ray Tracing

Table 1: some abbreviation with their description

Abbreviation	Description
HF	High Frequency
IRI	International Reference Ionosphere
COSPAR	Committee on Space Research
URSI	Union of Radio Science
TEC	Total Electron Content
vTEC	vertical Total Electron Content
GNSS	Global Navigation Satellite System
GIRO	Global Ionospheric Radio Observatory
Dst	Disturbance Storm Time
RT	Ray Tracing
MAPE	Mean Absolute Percentage Error
RMSE	Root Mean Squared Error

DOI: https://doi.org/10.61263/mjes.v4i1.132

1. Introduction

Communications at high frequencies are one of the most important basic branches of wireless communications, High-frequency waves propagate within the specified ranges. There are three types of propagation: propagation of waves in the ground, line-of-sight, and sky[1], There are numerous applicati ons for these waves, including long-range communications, radar detection, and radar tracking. Due to th e effects of sunlight and the changes that occur, what is called the ionosphere layers were created and formed[1]. It is a time-dependent, frequency-dispersive, isotropic, and homogeneous medium[2]. The first observations of the changes occurring and the formation of the ionosphere began in 1621[3]. The ionosphere's intricate structure creates a need to better portray and comprehend it for several reasons, man y disturbances and changes occur in the ionosphere layers and leading to an effect on temperatures, gases, frequencies, and altitudes. Therefore, Numerous models have been created that describe these changes. The most important of these, the International Reference Ionosphere (IRI) model a commonly accepted b enchmark for describing ionosphere parameters, which is promoted globally through the International Un ion of Radio Science (URSI) and the Committee on Space Research (COSPAR)[4].

these waves are exposed to many effects and factors, the most important of which are the effects of reflection, refraction, dispersion, and others, Ionospheric disturbances can affect High frequency (HF) rad io waves' propagation, These disturbances can weaken HF signals or even cut them off completely, which has major effects on wave propagation[5], To get rid of these problems, ray tracing is usually used [6]
In section 2 of this paper, we talk about the history of the ionosphere from the first observations to the most recent developments is briefly presented, some of its characteristics, and some effects, such as solar activity and geomagnetic storms.

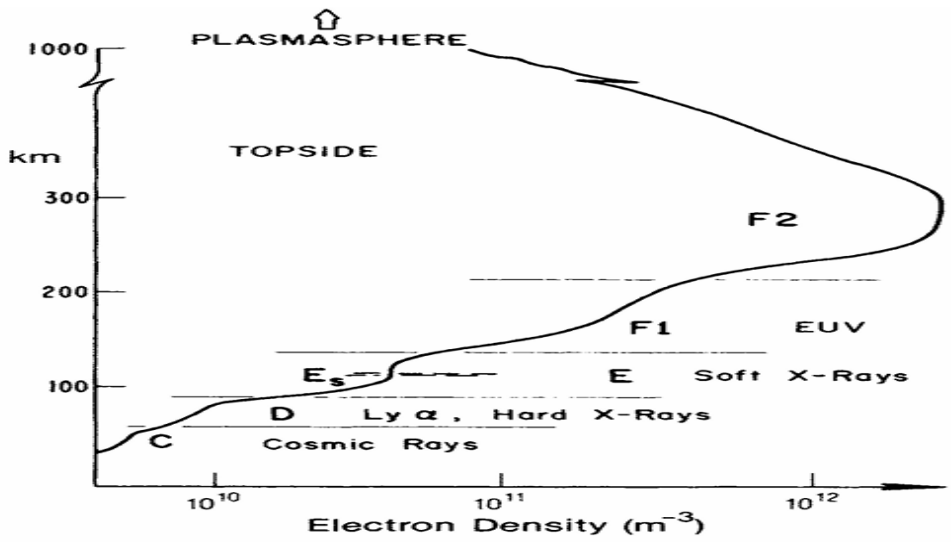

Figure 1: Structure of the ionosphere during A day in the middle latitudes for summer, along with the primary bands of cosmic and solar ionizing radiation [7].

Section 3 discusses the propagation models of high-frequency waves, Section 4 is the largest and most important part of the research, which discusses the empirical model that predicts the ionospheric par ameters' values, which is the IRI model, High-frequency waves are exposed to many factors while passing through the ionosphere and are affected by these factors, so in the section 5, we talked about a technique to reduce these effects, which is the ray tracing technique.

Table 2: Some of the Ionosphere characteristics

Ionosphere parameters	Description
FoF2 foF1 foE foEs	The F2, F1, E, and Es critical frequencies, respectively.
M(3000)F2 M(3000)F1	The maximum frequency factor that can be used for a transmission route of 3000 km by the layers of F2 and F1, respectively.
f_{min}	Minimum frequency at which vertical ionospheric reflections are visible.
hF2 hF hE hEs	Minimum virtual height for layers F2, F, E, Es, respectively.

2. Ionosphere

2.1 Ionosphere Historical

This section will explain the ionosphere's history using the initial observations and experiments that helped to create and solidify the idea.

2.1.1 Early Observations

Galileo Galilei found the visible aurora in the high atmosphere in 1621, and James Cork saw the same phenomenon in the Southern Hemisphere in 1773. This was the first evidence that the Earth's atmosphere had a conducting layer. Additionally, Olof Petrus Hiorter (1696–1750) noted that when he observed the Northern lights, a compass needle changed direction. While scientist Carl Gauss was observ ing the slight, consistent, and erratic fluctuations in the magnetic field of the Earth in 1839, it was the first indication that an electrically conducting layer might be present in the atmosphere [3].
We may trace the origins of wireless communications back to J.C. Maxwell's 1873 The Electricity and M agnetism Treatise. It served as a kind of foundation for the present theories of how electromagnetic waves propagate[8].

2.1.2 Marconi’s Experiment

When G. Marconi was able to transmit radio signals across the Atlantic in 1901, it was evident that the ionosphere existed. According to this experiment, the waves of radio waves were significantly more redirected over the surface of the Earth than could be explained by diffraction[9]. Utilizing a receivi ng antenna made of 120 meters of wire, Marconi sent radio communication signals from St. John's, Newf oundland, Canada, to Poldhu, Cornwall, England, spanning a distance of roughly 3500 kilometers. He ma naged to get messages across a distance of about 1000 kilometers throughout the daytime and up to 3000 km at night. Later, Marconi found out that, in contrast to the hundreds of kilowatts required at wider wavelengths, "Short waves" might provide reliable communication. Across the same power over thousa nds of kilometers.

2.1.3 Appleton and Barnett Experiment

Using the reflection across an electrically charged area of the atmosphere, E. Appleton was able to show that signals were detectable anywhere on Earth without LOS[8]. Appleton (1925) was the first to conclude the stratified nature of the ionosphere based on the observation that the height of reflection changed sharply near sunset.

The ionosphere plays a significant influence on electromagnetic waves, especially those with frequencies up to 300 MHz, by retarding and refractively altering them. The project known as Internation al Reference Ionosphere (IRI) was started in 1968 through the International Union of Radio Science (UR

SI) and the Committee on Space Research (COSPAR) due to its significance. The objective is to establis h and consistently improve a global standard for the terrestrial ionosphere's most crucial physical properties. The necessity for an ionosphere model for radio propagation purposes (URSI) and analyzing d ata (COSPAR) first spurred this demand, but the model has become increasingly significant for space weather purposes over time [10].

2.2 Ionosphere regions

Although much data on key frequencies was already available and ground-based sounders allowed for some in-depth investigation of the ionosphere in 1945, ionosonde data alone could not be used to solve problems. By 1970, many ionospheric events were understood to a relatively good degree[11]. There are several different zones or layers of electron density in the atmosphere because of the various molecules and atoms and their varying rates of absorption. These layers are denoted by the letters D, E, F1, and F2, and they are typically referred to as the ionosphere bottom side. In line with the ionospheric layer's design ation by each layer's maximal electron density, which is indicated by NmD, NmE, NmF1, and NmF2, respectively, the particular layer's penetration, plasma, or critical frequency is the lowest frequency of an electromagnetic wave required to penetrate it. It is represented by the symbols foD, foE,foF1, and foF2 [12].

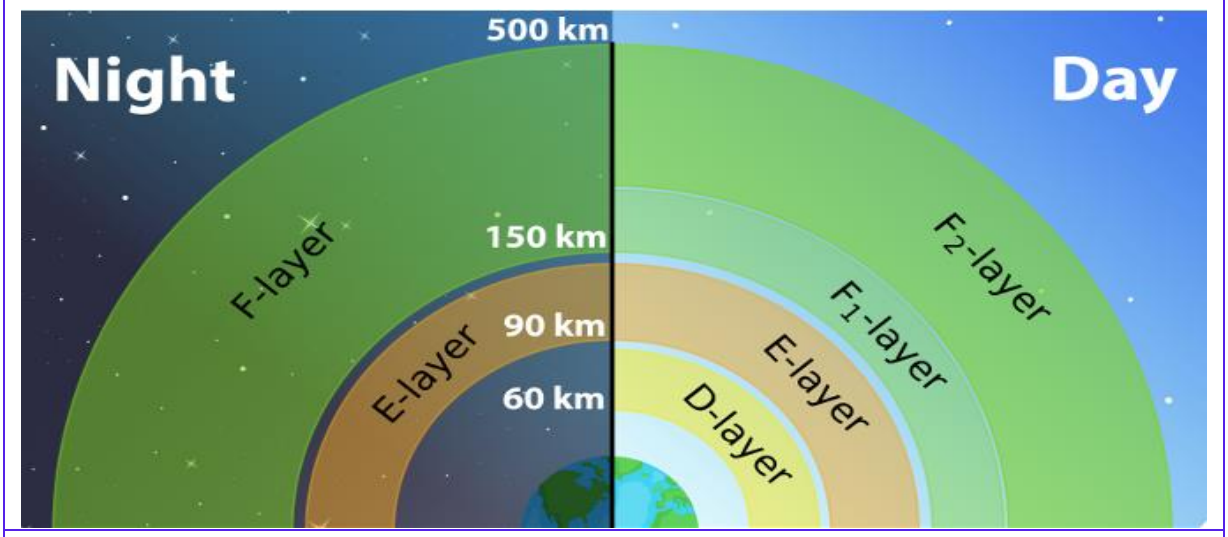

Figure 2: An example of the Earth's ionosphere ionization zones[13].

As shown in figure 2, The division of the ionosphere into 60–90 kilometers in the D region and 90–150 k m in the E region, and F region(150–1000 km) due to photo ionization and transport mechanisms. Additi onally, the F area is separated into the F1 region (150–220 km) and the F2 region (220-1000km) during the day [14].

2.3 Solar Activity

The scientific community uses a variety of terms to describe solar activity. The first is the degree of solar activity, which shows the strength of electromagnetic radiation from the sun, especially at extreme u ltraviolet (EUV), as well as solar X-ray (XUV) wavelengths. A second explains the phenomena of solar a ctivity, such as solar proton events and coronal mass ejections. Upon absorption of solar energy by the up per atmosphere of Earth, it causes heating, ionization, and dissociation.

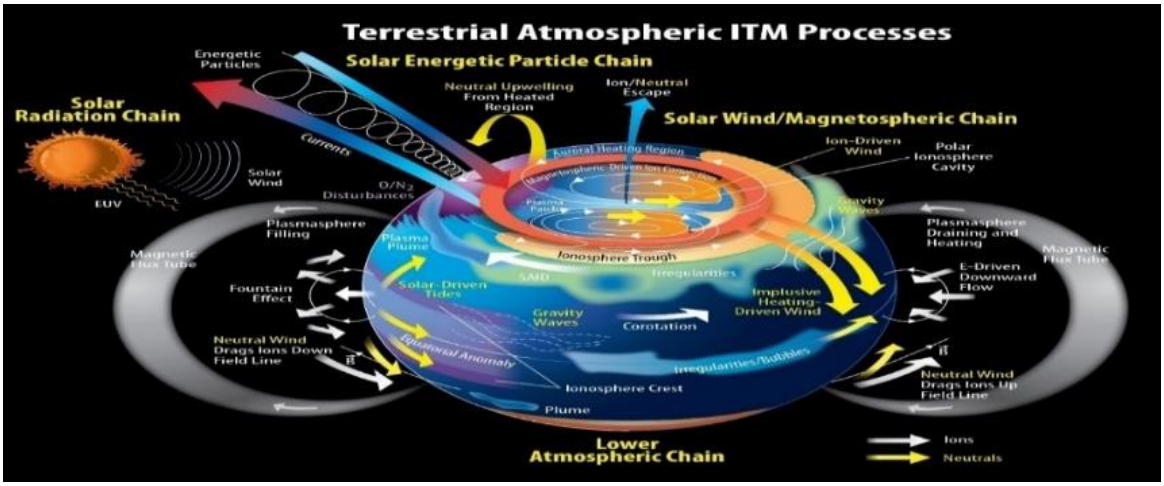

Figure 3: The complexity of Earth's ionosphere and high atmosphere [15].

The ionization process is the main source of the ionosphere's action to solar XUV. Notable varia tions in the quantities of ions and electrons, neutral winds, and electric fields in the ionosphere and tempe ratures are caused by fluctuating solar activity [16]. Long-term measurements of EUV and X-rays are required to forecast changes in the ionosphere's electron density with solar activity.

Under conditions of high solar activity, ionospheric measures like the TEC (total electron conten t) and foF2 exhibit impacts of saturation. Sunspot number has historically been regarded as the main indicator of solar activity [17].

2.4 Geomagnetic Storm

Coronal Mass Ejections (CME) are the name given to the ionization gases (plasma clouds) that travel through space from the Sun. They cause Earth's magnetic field lines to be disturbed, which results in geomagnetic storms. Sometimes, a high-energy solar wind stream is created as a result of intense solar activity, and it hits Earth's magnetic field. This results in geomagnetic storms that impact HF radio wave transmission and cause disturbances in Earth's ionosphere that can linger for a few hours, or perhaps two days, contingent on the severity of the storm and nature [18]. Of the phenomena about the solar wind and particles with high energy, and geomagnetic storms are arguably the most significant. They cause significant and worldwide ionosphere disruptions, but they also have an impact on the neutral atmosphere, which includes the troposphere and middle atmosphere. The development, duration, and strength of the i mplications of geomagnetic storms vary depending on the latitude and altitude. Their methods differ because they represent various aspects of geomagnetic storms. In the F2 layer, an ionospheric storm often shows up as changes in the electron concentration over a broad altitude range of roughly 200 km to 800–1000 km. The behavior of the total electron content (TEC) [19].

Ionospheric fluctuations throughout the world, as seen from ground-based locations, might appear chaotic during and after a geomagnetic storm. Changes in ionospheric density are seen to be both positive and negative [20], Numerous factors, including Season, solar activity, local time, geomagnetic latitude, s torm length, and storm onset time (the amount of time that passed after the storm began), storm severity, and pre-storm activity (Large storms rarely occur alone), affect the ionosphere's condition during a storm, The primary storm signature in the ionospheric F2 layer can be thought of as extended drops in NmF2 and the TEC throughout the storm's main phase, particularly at midlatitudes [21]. The night sector and the magnetic pole's longitude exhibit the strongest wind response. Increased ion drag-induced dissipation on the dayside is the cause of this preference for the night sector [25].

The following effects were found using the ground ionosonde data [21]:

(1) Traveling ionospheric disturbances that provide favorable storm effects.
(2) advantages brought about by a modification in the thermosphere wind's large-scale circulation.
(3) advantages brought about by the auroral ionization ring shifting equatorward.
(4) adverse consequences brought on by the neutral gas composition's disturbance.
(5) adverse consequences brought on by the trough zone shifting equatorward.

Compared to middle and lower middle latitudes, the stormy region of high latitude F is the most fluct uating due to magnetospheric activities, strong electric fields in particular, which are typically in existenc e when geomagnetic storms occur. The disruptions in high latitudes are significantly more severe than th ose in lower latitudes, The following is how the Disturbance Storm Time (DST) index is employed to spe cify the beginning, intensity, and multiple geomagnetic storm phases[22]:

- SSC, or sudden storm commencement, has been selected as a storm initiation indication. The drop in Dst (The magnetic field's strength) characterizes the storm's main phase, and the gradual return to calm conditions characterizes the recovery phase that follows.
- Dst ≤−100nT for at least four hours in a row was considered a strong storm state.
- a storm when Dst is less than -50nT, Intensity (Dst ≤−50 nT) from 1985 to 2005 is shown in Figure 4. N(e) divergence from the median values for quiet time is used to characterize the F region reaction to storm-induced disruptions, i.e., δN(e)

$$\delta n(e) = \{N(e)\mathrm{m} - N(e)\mathrm{med}\}/N(e)\mathrm{med} \quad (1)$$

Where:

- **N(e)m**: Measured electron density.
- **N(e)med**: Median (or modeled) electron density.
- **δn(e)**: Relative change or deviation in electron density.

Where the electrons' monthly median values concentration in the F region are measured, together with N(e)med and N(e)m[22]

Table 3 : Geomagnetic Storms [23]

	Number
Moderate (Dst <-50 nT, -100 nT)	409
Major (Dst < -100 nT < -250 nT)	153
Super (Dst < -250 nT)	22
Total (Dst < -50 nT)	584

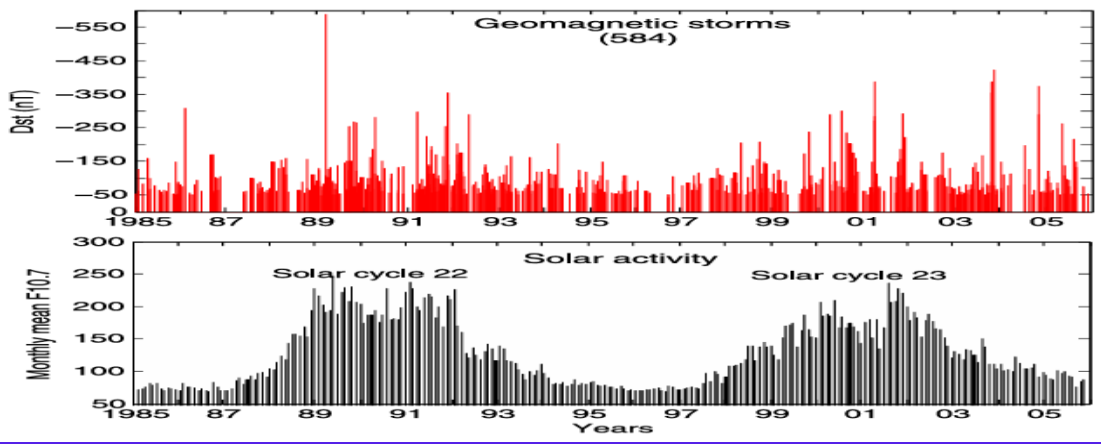

Figure 4: Geomagnetic storm frequency Furthermore, intensity (Dst ≤−50 nT) as a function of days from 1985 to 2005 is shown in (top), and the matching monthly average solar activity index, F10.7, is shown at the bottom (The compression causes the lines to appear differently) [23]

3 HF PROPAGATION MODES

3-kHz channels are used by several HF-range data transmission systems. The current trend in HF communication system development is to boost data transmission rates without expanding channel bandwidth. To function well under rapidly shifting channel conditions, it prompts a vigorous development of signal coding and processing techniques [24]. The new wideband HF (WBHF) family has enabled higher data rates, which have rekindled interest in HF radio after years of satisfying the need for low-cost, long-d istance communications without infrastructure. The mechanisms of propagation of sky waves have drawn the most attention in the research of HF propagation. Ground-wave propagation, however, can be a useful answer for some important operational requirements, which is why prediction capabilities for this mode of propagation should also be prioritized [25]. Different types of radio wave propagation occur, and each one has a unique process as shown in Figure 5. It can therefore be categorized as[26]:

- Ground (Surface) waves
- Space (Tropospheric) waves
- Sky (Ionospheric) waves.

Between 2 MHz and 30 MHz, three distinct propagation mechanisms can be identified:

- When stations can see each other directly, Line of Sight (LOS) propagation occurs.
- Ground wave propagation is how radio waves move across the Earth's surface
- Signals from the ionosphere are reflected during sky wave propagation.

Medium and HF display distinctive and specific characteristics in this mode. Sky wave propagation makes it possible for stations on different sides of the planet to communicate with one another over the horizon [27]. For long-distance communication, HF radio waves are essential due to their inexpensive terminal hardware costs, sufficient transmission capacity, acceptable signal quality, and low power consumption.

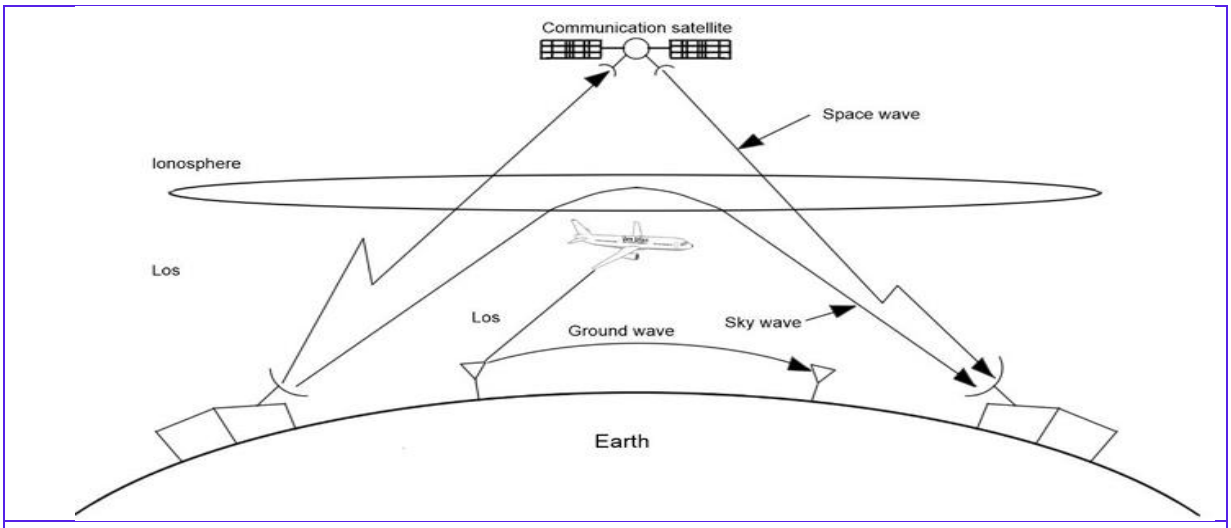

Figure 5:The way radio waves travel via the ground, ionosphere, and space[27].

4 International Reference Ionosphere (IRI)

4.1 Overview of IRI

The International Reference Ionosphere (IRI), a commonly accepted standard for describing ionosphere parameters, is promoted globally through the Committee on Space Research (COSPAR) and the International Union of Radio Science (URSI) [28]. COSPAR's primary goal is to provide a broad explanation of the ionosphere's role in the terrestrial environment so that the environmental influences on spacecraft and experiments may be evaluated. For URSI, for research and use, a reference model that describes the background ionosphere is essential. It is related to radio wave propagation [4].

The model's initial iteration that was widely utilized was IRI-78 (Version No. 5). The shift from a ta bular model (profiles for usual circumstances) to a genuinely global model. Before the end of 1980, a new version was anticipated, IRI-80. The next major event was the publication of Version No. 9 of IRI-86, the initial edition to be accessible on diskette and online for use on PCs, after a six-year cycle of advancemen t. The IRI computer program's November 1990 edition, IRI-90 (PC application: Version 11.), contain ed neutral temperature using the latest CIRA stands for COSPAR International Reference Atmosphere. T his was followed by the November 1991 release of Version 12 of the IRI software [29]. The model has be en continuously improved using newer data and improved modelling methodologies, resulting in the public publication of many important iterations, For instance, IRI-78 (Rawer and associates (1978)), Bili tza's 1986 IRI-85, IRI-1990 (Bilitza 1990), Bilitza (2001) cited IRI-2000, and IRI-2007 (Reinisch and Bil itza (2008))[30], look to table 4 describe IRI models from 1968 to 2016.

Table 4: Lists the key turning points in the IRI project's brief history. Note: Rawer et al. (1978b) also describe IRI-79 [4].

Year	Event (reference)	Description	Database
1968	COSPAR establishes an IRI Working Group.	WG participants They are mostly from the community of space, with K. Rawer as the chai r (rocket and satellite measurements)	
1969	URSI joins the initiative of IRI.	Members of the ground observation community who have joined the WG	
1975	A collection of tables (RIRI-75; Rawer et al., 1975)	Equatorial, low, and mid-latitude representative values	Ionosonde, ICS, AEROS
1978	IRI 79: Special Report on UR SI (Rawer and associates, 1 978)	IG12 with foF2; global coverage utilizing CCIR charts for peak attribute s, adjusted for foE and foF1	Global ionosonde network
1981	WDC-A-STP Rep. IRI-79 (In 1981, Rawer et al.)		
1986	IRI-86: floppy disk for PC (Bilitza (1985, 1986))	• Better Ne in low-latitude regions • Te, Ti models worldwide	ICS data, ISIS-1, -2, AER OS-A, -B, AE-C, -D, and -E
1990	IRI-90: Report of the NSS DC (Bilitza in 1990)	• URSI maps for the foF 2 • Improved NmE model	• Additional worldwide ionosonde data • Data with incoherent scatter (ICS)
1995	IRI-95: online (IRI Web) (Bilitza (1997))	• Advances in low latitud es	DE-2 data
1999	Resolution of URSI	IRI is acknowledged as the global ionosphere standard	

2001	IRI-2001
	(2001's Bilitza)
		• Two fresh choices for the Ne D-D-region
		• New F1 and B0, B1 models
		  • STORM model
		  • New model for Te
		  • IGRF update
			• Rocket compilations
			• Ionosonde network
			• Storm-time ionosonde data
			• Intercosmos 19, 24, 25

2007	IRI-2007 (Reinisch & Bilitza 2008)	• Ne topside has two new possibili ties. • A novel model of ion compositio n • The spread-F occurrence model	• TS: ISIS 1, 2, Alouet te 1, 2 • Intercosmos 24, AE-C,-E • Data about the Brazili an ionosonde
2012	IRI-2012 (D. Bilitza and others, 2014)	• New model for BO and BI • Auroral boundaries model • Auroral storm-time model foE • Te solar activity dependence • FLIP ion composition model • NRLMSIS00, IGRF-11	• Worldwide digisonde data • TIMED/GUVI data • TIMED/SABER data • Satellite database • FLIP normalized to IRI-Ne • Update to the latest version
2014	ISO Certification	IRI is certified as an ISO standard for the ionosphere	
2016	IRI-2016 (Bilitza, D. et al. (2017))	• 2 new models for hmF2 • Ion composition at low F10.7 • Real-Time IRI (IRTAM)	• Digisonde; Radio Occ. • C/NOFS data • Global Digisonde Network

IRI, or the International Reference Ionosphere, is a technical specification (TS) of the International Organization for Standardization (ISO) [31]. One advantage of IRI is that it is an empirical model, which means it is not reliant on a conceptual comprehension of the mechanisms that produce the ever-changing ionospheric plasma[30]. In contrast to theoretical models, the IRl aims to serve as a useful reference by integrating recognized scientific findings without depending on theoretical assumptions[32]. Monthly averages of the present range of ionospheric altitude are between 50 and 1500 km, are provided by IRI for ion composition, ion temperature, ion drift, electron density, and electron temperature. The description of the monthly quartiles and deciles is also being tried to incorporate a gauge of the month's io nospheric variability [31].
Empirical models' heavy reliance on the underlying database is one of their drawbacks. In areas and eras that the database does not adequately cover, the model's reliability will be diminished [30].

The IRI Working Group has grown to include 58 specialists over the years, look to figure 6. Providing a global presence and a balanced representation of the several ground and satellite approaches utilized to gather ionospheric data. This robust coverage has been technically and internationally beneficial to the IRI project, as it has facilitated the acquisition of all important ionosphere ground and space data sets[33].

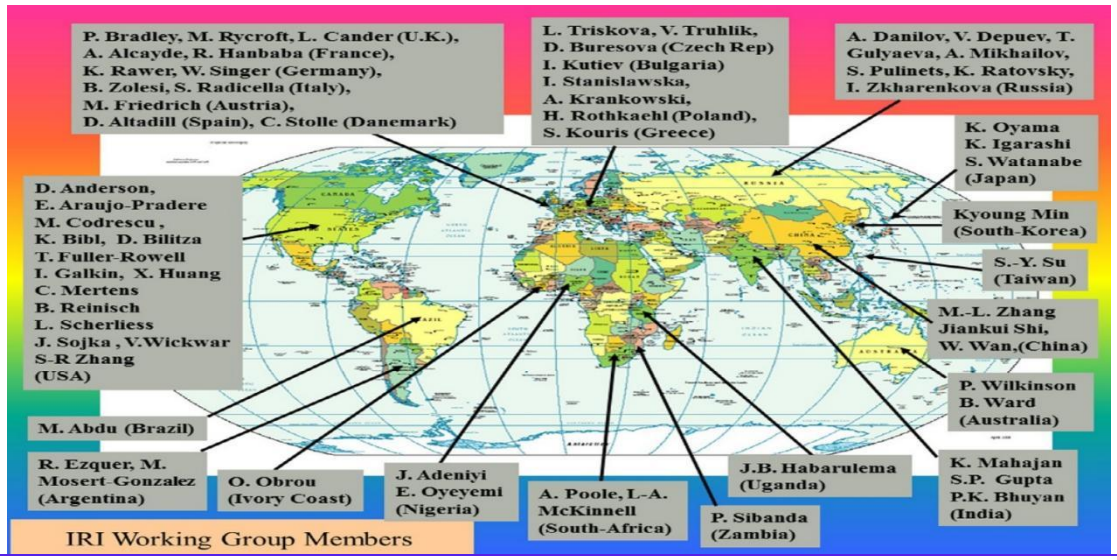

Figure 6: Members of the International Reference Ionosphere Working Group of URSI/COSPAR are distributed throughout the world [33]

4.2 Modern IRI models

(Bilitza & Reinisch, 2008) [31] IRI-2007, highlighting the key modifications made with this iteration. These consist of (1) There are two new alternatives concerning the electron density on the upper side: the NeQuick topside model (IRI-2007b) and an adjustment factor for the model from 2001. These options offer better results and will facilitate a more seamless transition to plasma spheric models. (2) A novel concept for the creation of upper-side ions, (3) the addition of a model for the likelihood of diffuse F occurring for the first time, (4) an electron density model for the auroral E zone using Neural Nets, (5) A simulation of the electron temperature of the plasma, and (6)According to the most recent model of the International Geomagnetic Reference Field (IGRF), magnetic coordinates are determined by considering their fluctuations due to secular magnetic field variation.

(Bilitza et al., 2014) [33], in this paper, by using updating and assimilation techniques, IRI were combined with real-time data and based on the modeling efforts of the previous version IRI-2007 to make the model successful and include many important improvements and additions, these improvements do not

include only electron density, also improved on the electron temperature as well as the composition of ions.

(Bilitza, 2018) [4]In this paper, the important changes and improvements listed in IRI-2016 are discussed, and how they affect the IRI prediction of the ionosphere parameter. Two new choices for high electron peak height are included in IRI-2016. (Data from radio occultation and digitization) and a better representation of the ion density on the upper side in various solar activities. From the small changes about the use of solar indicators, the limits of the permissible solar index F10.7 were extended from (85-200) in IRI-2012 to (65-260), and the computer program was accelerated. The results of this version were more accurate and reliable.

(Bilitza et al., 2021)[34]In this paper, several new inputs have been added to the model, including:1. A model of the electron density in the D region based on a simple ion chemical model corrected using radio propagation data, 2. A new model to represent the peak frequency of the plasma F2, including storm and ionospheric effects by Shubin and Deminov, 3. A model by Blanche and Atadil for hmF2 that represents the effects of ionospheric storms on the F2 atomic height based on ionosonde data, 4. Improved representation of the variation of solar activity for the upper electron density, 5. A new and accurate model for the ion temperature has been added based on a large database at the sites.

4.3 Validation of the IRI Model

New information from strong incoherent scattering radars, the global network of ionosondes, and o n-board in situ instrumentation from Numerous rockets is added. Due to the extra data and studies, such as IRIs from 2007 to 2020, 2012 to 2016, and 2016, that have become available within the last 20 years. T wo more F2 peak height hmF2 model choices are included in the IRI model. Additionally, it provides a m ore precise approximation of the ion densities at the top, especially at extremes of solar activity. The prim ary input components are altitude range, time, date, location, and solar, magnetic, and ionosphere indices. [35].

A model is verified by comparing it with experimental data to determine how well it predicts the process it was meant to estimate and the design objectives. The electron in this instance of the IRI model and ion temperatures were estimated using well-accepted metrics from the literature. Two metrics are It is commonly practice to assess precision using Mean Absolute Percentage Error (MAPE) and Root Mean Squared Error (RMSE)

$$RMSE = \sqrt{\frac{\sum_{t=1}^{n}(A_t - F_t)^2}{n}} \quad (2)$$

$$MAPE = \frac{\sum_{t=1}^{n}\left|\frac{A_t - F_t}{A_t}\right|}{n} \times 100 \quad (3)$$

where n represents the overall number of cases., Ft is the predicted value, while at is the actual value.

The three online versions of the IRI model (IRIs from 2007, 2012, and 2016) and the Higher altitude ele ctron and ion temperature sub-options have been updated. The CS values determined using three online v ersions of the model's temperature profiles were compared with the CS values observed using the ISR te mperature readings to validate the model. In general, the estimates in the IRI-2016 version are superior to those in the previous versions[35].

4.4 IRI Drivers

A model's external drivers are frequently significant since they allow the model to accurately sy mbolize the circumstances of the ionospheric. The IRI is computed from ionospheric, magnetic, and solar measurements using these ionospheric, magnetic, and solar indices[10].

4.4.1 Solar Indices

By using indices that are based on measurements, the traditional method is used. In IRI, we use in dications that are ionospheric, magnetic, and solar. Table 4 enumerates the ionosphere and solar indices u sed in the various IRI sub-models.

Many early ionospheric models used the sunspot number R as their index, which has to do with the quant ity of spots and clusters of spots on the sun. There are still some older IRI sub-models that use this index. The average during a 12-month period of R (abbreviated R12) is frequently used in the models [4]. Regar ding models such as IRI that were created using the antiquated R index, this must be considered; for IRI, this is achieved by the use of the revised index with a 0.7 scaling factor. The ITU advises characterizing the sun activity of their well-known CCIR (1967) model with solar index R12 for Maximum Frequency f or F2 Layer at 3000 km (M(3000)F2) and foF2.

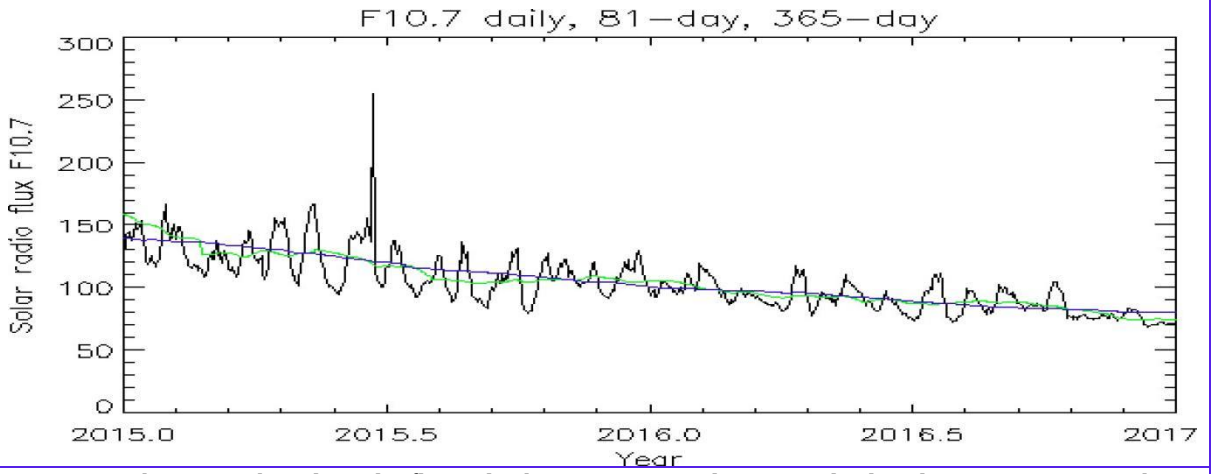

Figure 7: Changes in the solar radio flux index between 2015 and 2017 are displayed in Figure7 F10.7. This shows the 365-day average (blue curve), the 81-day average (green curve) of three solar rotations, and the daily index (black curve) [4].

4.4.2 Equivalent indices

The index or indexes that drive the model are adjusted to provide an equal index once the data and the model agree. This approach of station-specific modeling is widely utilized. For modeling at the regional o r worldwide level, the space between stations has to be incorporated using an interpolation or averaging method. IRI has been merged with a number of data sources for this. The majority of efforts have been directed at achieving equal indices of the F2peakheight and density, respectively, due to the significant significance that the R12 and IG12 indices play in deterring mining of ‘these two variables. [36] used glo bal ionosonde data between 1986 and 1989 to generate comparable IG indices, improving IRI ionospheri c adjustments altimeter measurements. The technique of equivalent indexing has also been effectively applied to other models, such as IRI. Similar to the method used by [37] for the IG12 variation in IRI, [38]significantly improved the NeQuick model's performance by altering the model's F10.7 version with GPS TEC maps. Based on the findings, this is a very promising path., and IRI is expected to get better in the future as these methods are improved [4].

4.4.3 Ionospheric Indices

The global index of Ionosonde (IG) is created by adapting the CCIR (1967) model's solar cycle representation of foF2 to midday for observations of F2 ionosondes. The IG index's benefit is that it incorporates dynamic affects that solar indices do not because it is based on ionospheric data. Due to the f

act that Regional differences are balanced by the global index, it has been shown that foF2 has a stronger correlation with IG's 12-month running mean (IG12) as opposed to its monthly value. Following that, IRI models foF2 using IG12. When considering hemispheric IG indexes, in 2018, Brown et al. discovered tha t the monthly indices outperform the 12-month running means. In particular, they demonstrated that the IRI model performs nearly twice as well when monthly hemisphere indices are used [10]. If just R12 is in put, IG12 is automatically updated using IG12 and R12's long-term correlation function , and vice versa [39].

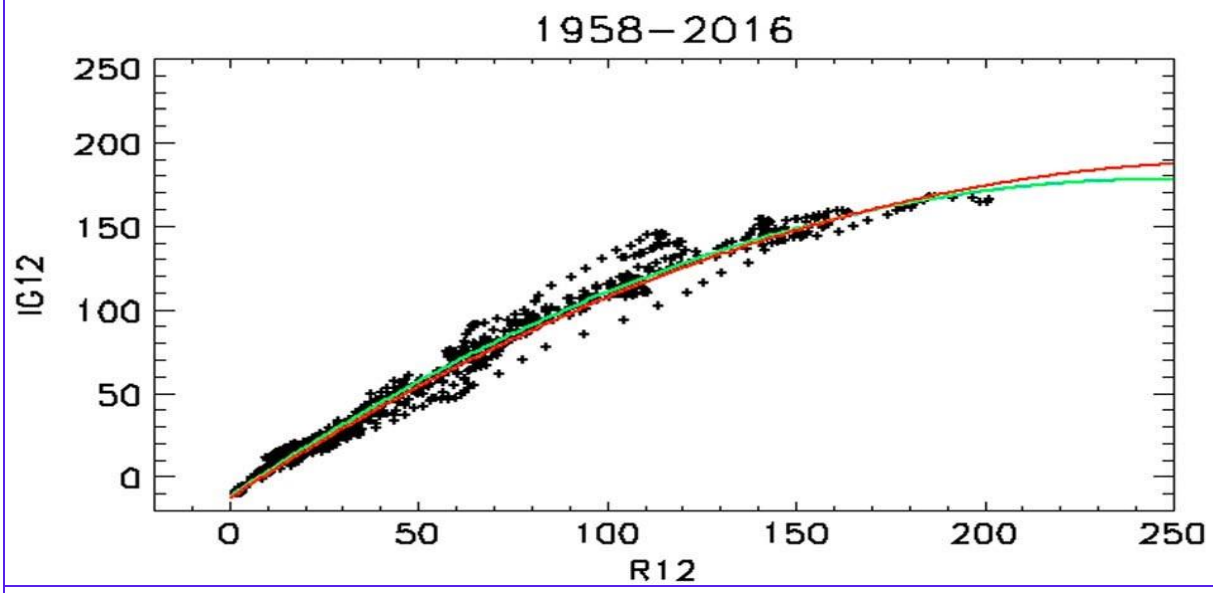

Figure 8: shows the curves fitted and the correlation between the indices IG12 and R12 (+) from 1958 to 2016 [39].

4.4 IRI in Real Time and the IRTAM Approach

In the last few years, to enhance the IRI output, various data-assimilation approaches have been used. Th e objective is to describe the ionospheric weather conditions by ingesting real-time measurements, as opp osed to using the portrayal of climate offered through the conventional IRI model.[36]. utilized global ionosonde information between 1986 and 1989 to generate comparable IG indices[37],[40], [41], and [42], to determine an appropriate IG12 in order to modernize the European region's IRI model; Recently, they upgraded their process by using vertical total electron (vTEC) values as well[43]. By including iono sonde F2-layer peak parameter values, Pezzopane et al. and Pietrella et al. initially calculated an efficient sunspot number that the Simplified Ionospheric Regional Model uses, They subsequently used an interpo lation approach to incorporate the entire profile of electron density captured by ionosondes into IRI [44] .

IRTAM, or IRI Real-Time Assimilative Modelling, IRI Real-Time's most advanced model, was created by [45] that incorporates The IRI model incorporates digital data from the Global Ionospheric Radio Obs ervatory (GIRO) network. The F2 peak plasma frequency foF2 models from CCIR [1967] serve as the fo undation for the IRTAM technique and throttle factor Maximum Frequency for F2 Layer at 3000 km (M (3000)F2), which is employed in IRI. IRTAM describes the global environment using the CCIR set of fu nctions and geographical variance in the discrepancy from the digisonde measurement to the prediction o f the foF2 IRI [39].

4.6 Previous IRI studies

(Timoçin et al., 2018)[46] In this paper, the accuracy of the IRI-2016 ionosphere prediction of foF2 values was compared with the actual values In various latitudes throughout the geomagnetic storms of 19 89. The IRI-2016 model was used and its performance varied from season to season depending on the changes in magnetic activity. The IRI-2016 estimated foF2 values were compared with the values measured by ionosonde during disturbed periods by calculating the root mean square errors and percentage deviatio ns (RMSE). The researchers found that the IRI-2016 forecasts for F2 are not accurate. significantly from those quantified by ionosonde stations during geomagnetically disturbed periods. The seasons and latitu des affect this deviation, with the largest deviations occurring at high latitudes, During the June period, the smallest deviations occurred, while during the December period, the percentage deviations were at their largest values.

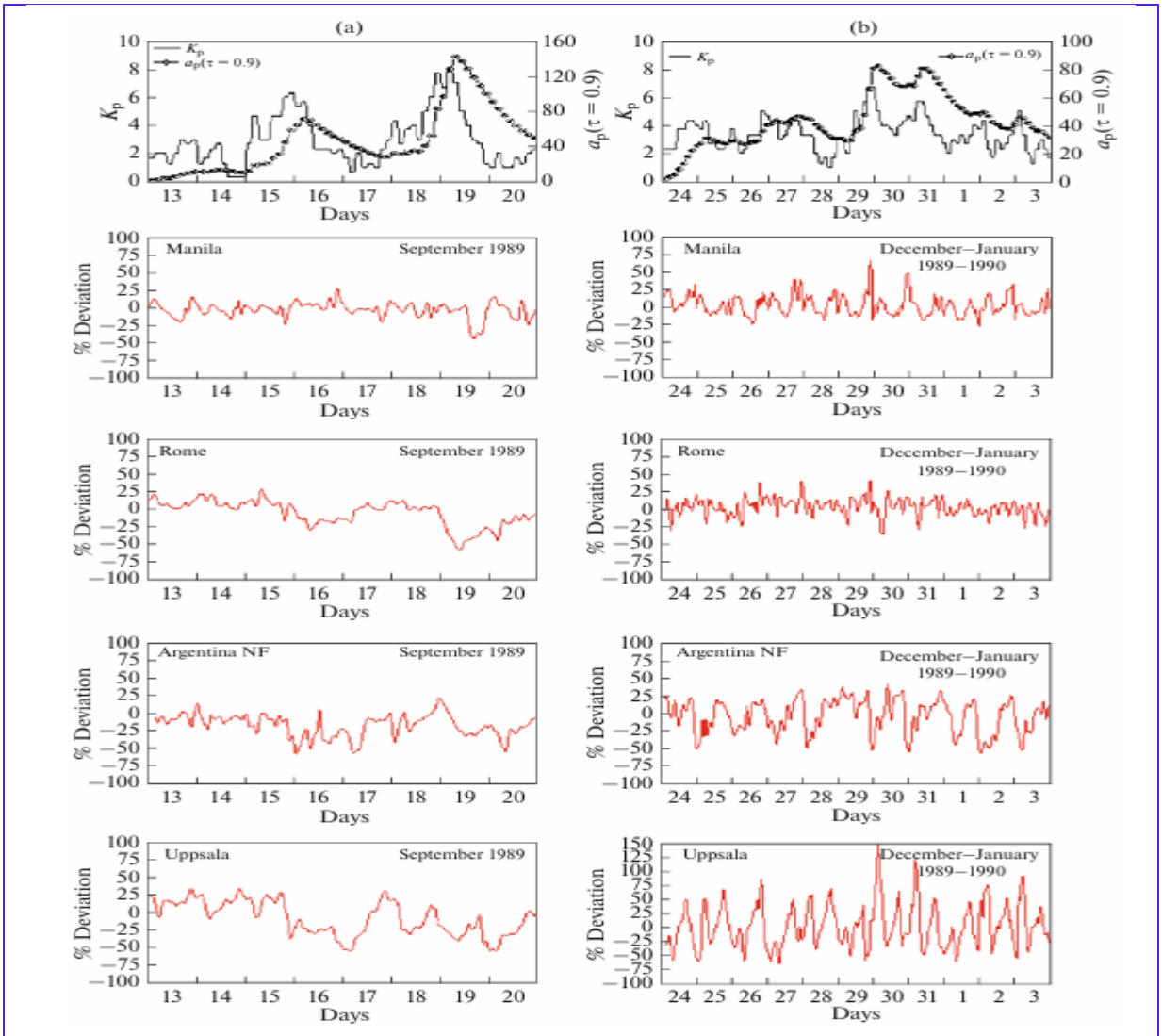

Figure 9: The planetary geomagnetic indices' daily variations (K_p, a_p (= 0.9)) and how percentage deviations behave for several stations of ionosonde (a) between 13 - 20 September 1989; (b) between 24-03 December 1989, and January 1990[46].

(Fagre et al., 2019)[47] In this paper, various the foF2 and hmF2 models choices' effects in the 2016-IRI and The numerical ray tracing method is used to assess to the HF ray's ground range and height of reflection pathways in order to determine their spatial variation. The research methodology involves hi gh-frequency wave ray tracing in the ionosphere taking into account the complex nature of magnetized plasma and magnetic field's impact on propagation. Spherical coordinates were used in Hamiltonian equations for ray tracing techniques. The results showed differences in reflection height and ground range with large differences observed in certain regions. Different model settings led to different values of R, h due to differences in electron density, refractive index, magnetic field, etc.

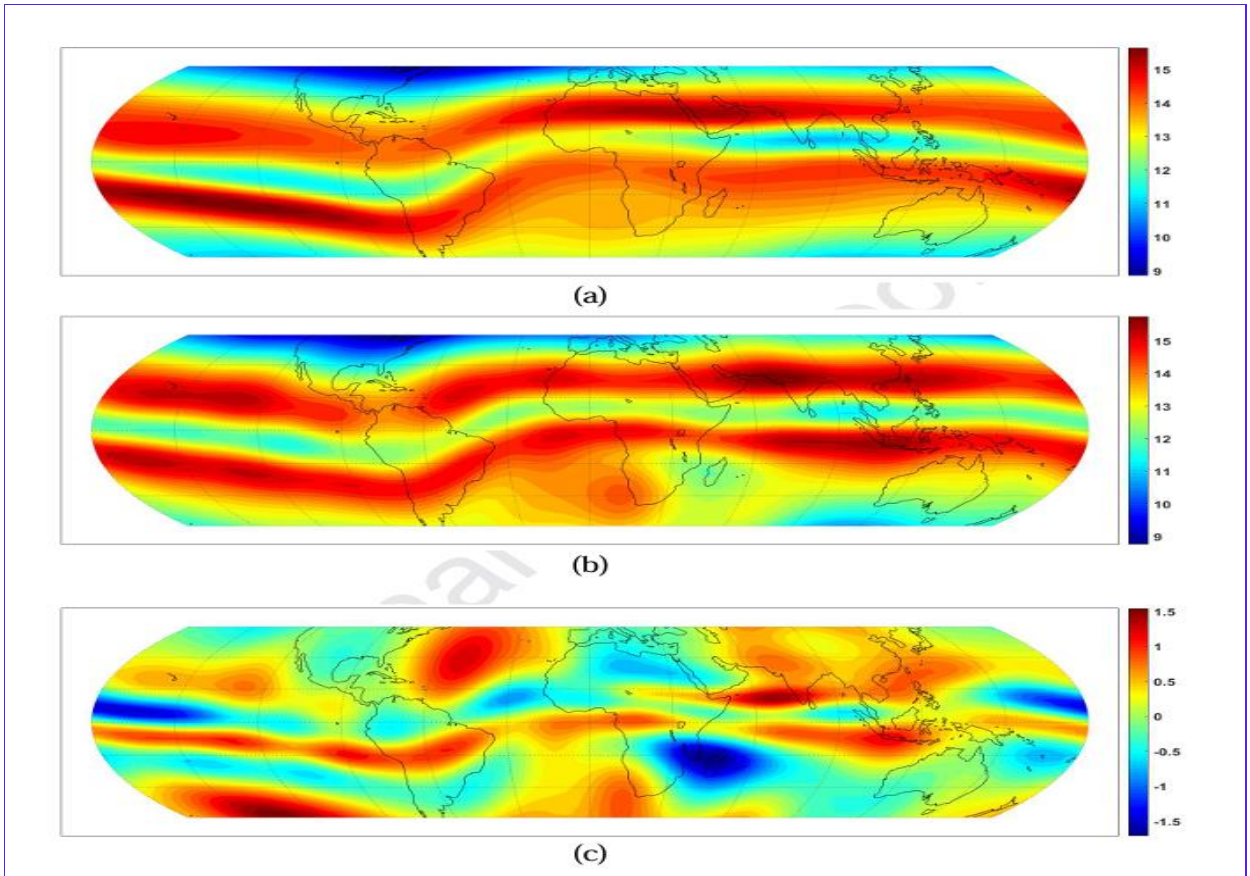

Figure 10 : foF2 [MHz] acquired with both of the IRI 2016 optional models: (a) URSI and (b) CCIR (c) Variation in [MHz] between foF2 readings obtained using the hmF2 M(3000)F2 model between the CCIR and URSI mo dels using IRI-2016. On April 26, values for 12 LT were obtained.

(Al-Shallal & Al-Ubaidi, 2020)[18], This paper aims to enhance the reliability of high-frequency communications during blackouts in periods of strong geomagnetic storms, where the highest frequency v alues that can be used for the ionosphere's F2 layer are calculated using ionosonde observations and contr asted with the IRI_2016 model's estimated Maximum Usable Frequency (MUF) for the same layer. The results of this research were that the observed and projected MUF values during powerful storms do not c orrelate well (the relationship is non-linear). The colder the atmosphere, the greater the ionosphere's ioniz ation and electron density, and thus the MUF values increase during the day more than at night.

(Kim & Kwak, 2024)[48] This paper aims to verify The IRI-2020 model's validity during severe geomagnetic storms in the Nort-East Asia region. The hmF2 and foF2 readings of six Japanese and Korea n stations were analyzed, and the vTEC data were examined. Global Navigation Satellite System (GNSS) receiver data from three locations in Korea and 2 sites in Japan were also obtained using the model of IRI

-2020. The model's inability to precisely compute the absolute variations in foF2 that occurred during pos itive storms were the outcome, However, it consistently calculated that positive ionospheric storm had a l arger electron density than calm days, especially in values of vTEC. Likewise, in the event of negative st orms, it forecasted a lower electron density than on days when everything was quiet, but was unable to re cord the peaks of wave-like disruptions that undergo quick changes. For hmF2 values, the model comput ed coordinated values for both positive and negative storms. IRI-2001 performed better for positive storm s, and IRI-cor2 performed better for negative storms, but needed significant improvements when consider ing absolute values.

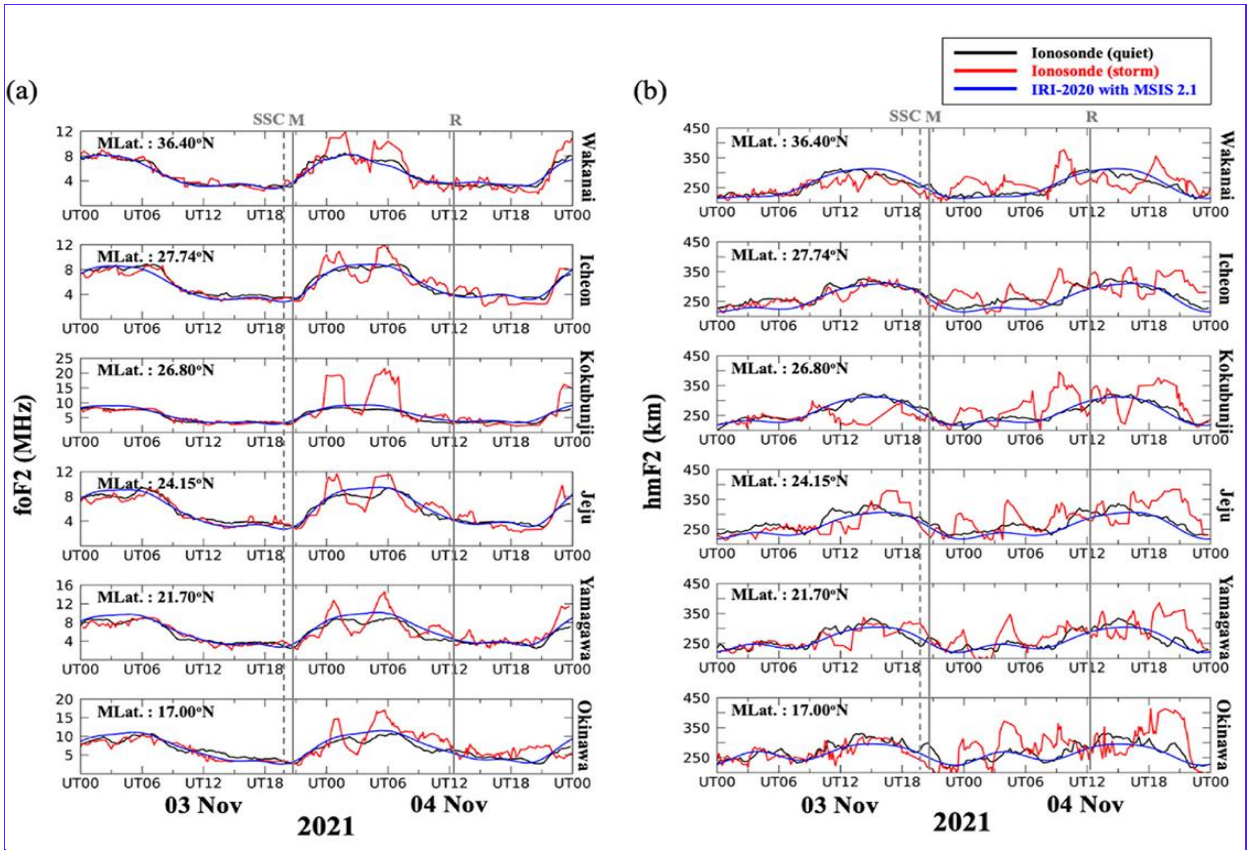

Figure 11 : Of the six ionosonde stations, the foF2 values (a) and hmF2 values (b). during the November 3rd and 4th, 2021, G3 geomagnetic storm events. The panels are positioned starting from the top panel in order of increasing latitude, Using solid black lines

(Height, 2024)[49]This research presents a new method for determining the F2-region peak electron density height (hmF2) in the ionosphere based on the physical relationship between hmF2 and the M(3000)F2 propagation factor The method incorporates seasonal and diurnal variations using a linear regression approach Data from six ionosonde stations in East Asia were used for model development and validation The proposed model demonstrates higher accuracy compared to existing IRI models with significantly lower root mean square error and relative error values The simplicity and precision of this model make it a useful tool for HF communication design and ionospheric studies

(Ubaidi et al., 2024)[50]The study titled "Disturbances of Ionospheric Total Electron Content during Great and Severe Geomagnetic Storms above Iraq and Surrounding Areas" investigates how intense geomagnetic storms affect the ionosphere over Iraq. Focusing on the major storm of October 28–30, 2003,

researchers analyzed Total Electron Content (TEC) data from the USTEC database and geomagnetic indices like Dst. Findings revealed a strong correlation between Dst index variations and TEC fluctuations, with daytime TEC values generally higher than nighttime ones. However, anomalies were observed when the storm persisted for several hours during the day, indicating complex ionospheric responses. These insights are crucial for enhancing the reliability of satellite-based communication and navigation systems in the region during geomagnetic disturbances.

(Hazim & Al-Ubaidi, 2025)[51]The study titled "Investigating the Effect of Sudden Stratospheric Warming on the Ionosphere above Basrah City" examines how sudden stratospheric warming (SSW) events during winter impact ionospheric parameters over Basrah, Iraq. Utilizing the IRI-20 model and data from 2014 and 2019, the researchers analyzed seven SSW events, focusing on total electron content (TEC), and critical frequencies foE and foF2 of the E and F2 layers. Findings indicate non-linear relationships between stratospheric temperature peaks and ionospheric responses, with notable daytime increases in TEC during SSW events, peaking in the afternoon and declining after sunset. Variations in foE and foF2 were also observed, influenced by changes in thermosphere composition, temperature, winds, and dynamo activities in the E and F regions.

(Seba & Poedts, 2025)[52]This study evaluates the IRI-2020 model's accuracy in predicting ionospheric parameters like foF2 and MUF(3000)F2 using data from multiple global ionosonde stations, revealing consistent overestimations, location-dependent accuracy, and the influence of solar activity, thereby emphasizing the need for regional calibration to improve its reliability in HF communication applications.

Table 5: Comparative Review of IRI Model Accuracy and Performance

Reference	Model Used	Main Focus	Methodology	Key Findings
Timoçin et al., 2018	IRI-2016	foF2 accuracy during 1989 storms	RMSE & % deviation vs ionosonde	IRI-2016 less accurate in disturbed conditions; deviations varied by season and latitude
Fagre et al., 2019	IRI-2016 + Ray Tracing	HF ray path and reflection height	Numerical ray tracing in spherical coordinates	Significant regional differences due to model settings (electron density, refractive index)
Al-Shallal & Al-Ubaidi, 2020	IRI-2016	MUF reliability during storms	Comparison of observed vs. model MUF	Poor correlation, non-linear relationship; MUF affected by temperature and ionization
Kim & Kwak, 2024	IRI-2020, IRI-2001, IRI-COR2	IRI model validation in NE Asia storms	foF2, hmF2, vTEC analysis using GNSS & ionosondes	IRI-2020 showed trends but missed absolute values; IRI-2001 best for positive, COR2 for negative storms
Height, 2024	Custom Linear Model vs IRI	Estimation of hmF2 using M(3000)F2	Regression using East Asia ionosonde data	Proposed model outperformed IRI models; more accurate and simpler for HF planning
Ubaidi et al., 2024	Empirical + USTEC Data	TEC variations during major storms over Iraq	Analysis of TEC vs. Dst index	Strong TEC-Dst correlation; complex responses during prolonged daytime storms
Hazim & Al-Ubaidi, 2025	IRI-2020	SSW effects on ionosphere over Basrah	Analysis of 7 SSW events (TEC, foE, foF2)	Non-linear effects; increased daytime TEC and changes in foE/foF2 due to thermospheric dynamics
Seba & Poedts, 2025	IRI-2020	Global accuracy of foF2 and MUF(3000)F2	Comparison using multi-site ionosonde data	Overestimation by IRI-2020; performance depends on location and solar activity; regional calibration needed

4 RAY TRACING

In contrast to the radio wavelength, ionospheric composition at a vast scale cause's refraction and reflection, which are the primary causes of Tracing HF radio waves in the ionosphere. The determined gr ound range, height of reflection, and phase path parameters, and the collective route allow for an effective evaluation of the tracing results. Ray tracing can be used in experimental research on direction-finding an d radar devices that are located beyond the horizon, as well as in the prediction of HF broadcasting or communication systems and in the management of operation frequency and power. Accurately tracking the ray using a realistic ionospheric model is crucial to the success of these beyond line-of-sight systems. two primary forms of ionosphere ray tracing: analytical and numerical. The theoretical underpinnings, as well as several applications and methodologies, of ray tracing have been examined and explored by Bennett et al. [2004]. Overall, Jones's program is likely the most used numerical ray-tracing program [53].

The basis for the ray tracing method is the application of ray optics to solve Maxwell's equations in the hi gh frequency region. The ray tracing approach thus gives predictions for time delays, arrival/departure an gle, and route loss, which is a technique for modeling generic propagation. The method of ray tracing doe s not provide straight forward formulas for calculating path loss, in contrast to theoretical and empirical models. It is a computer program that solves Maxwell's equations numerically [54]. The ray tracing problem can be quickly and easily solved using Snell's law (shown in Figure 13), which provides a quick run-time solution without ignoring any physical properties in the ionosphere's 3D grid structure. Snell's law states that a ray is reflected or refracted when it reaches An incidence angle on a plane [2]**.**

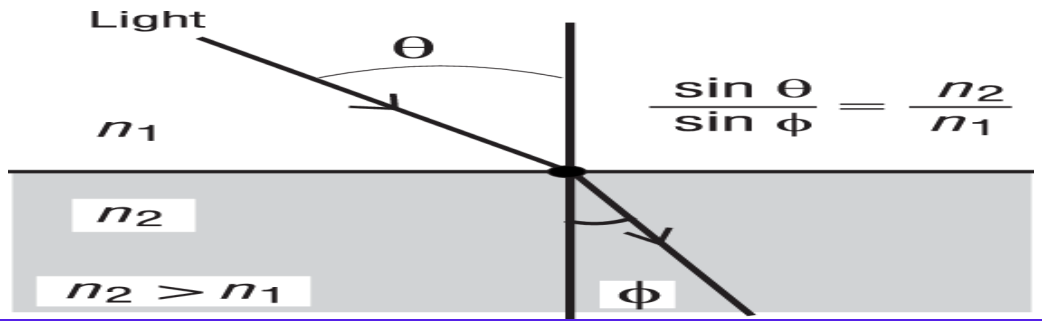

Figure 12: Refraction and Snell's law [55]

5.1 The ray concept

Our daily encounters with sunlight make the ray notion very obvious. When sunlight enters a room through a huge (about wavelengths) opening in a wall, we may see the ray traveling in a straight line. The following is a summary of the ray idea for radio propagation modeling utilizing ray tracing[54]:

1) In a homogeneous medium, a ray moves in a straight line.
2) It complies with the rules of diffraction, reflection, and refraction, shown in Figure 14.
3) Energy is carried by rays. It makes more sense to think of a ray as a tube that contains and distributes energy around the core ray

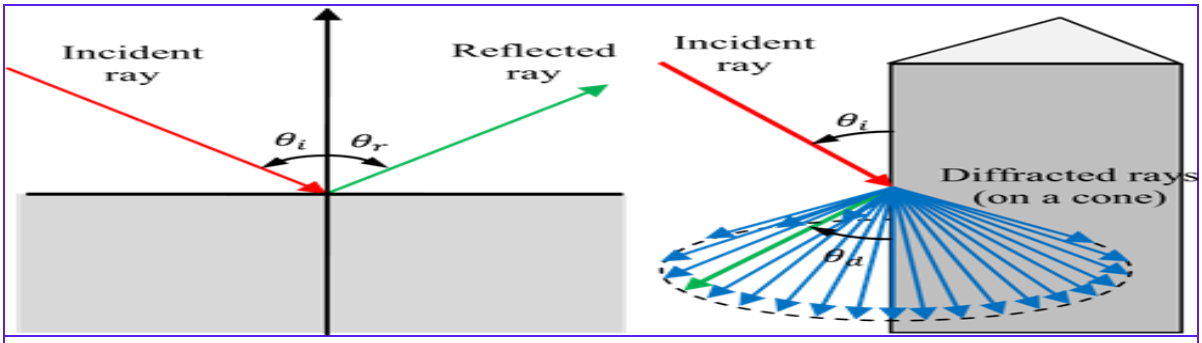

Figure13: shows the rays that are diffracted from an edge (right) and the left-hand reflected bea m from a planar contact between two different media. Keep in mind that there is A spectrum of rays that are diffracted (on a cone) rather than a single reflected ray [54].

Table 6: Ray-Tracing Equation Symbols[57]

5.2 Previous ray tracing studies

(Darwin, 1895)[56] This report was published in 1975 by Jones and Stevenson. They used the Fortran language to describe the three-dimensional path of rays. The wave path is traced through the ionospheric model, which integrates Hamilton's four-dimensional equations (One temporal and three spatial).

$$\frac{dr}{d\tau} = \frac{\partial H}{\partial k_r} \quad (4)$$

$$\frac{d\theta}{d\tau} = \frac{1}{r}\frac{\partial H}{\partial k_\theta} \quad (5)$$

$$\frac{d\varphi}{d\tau} = \frac{1}{r\sin\theta}\frac{\partial H}{\partial k_\varphi} \quad (6)$$

$$\frac{dk_r}{d\tau} = -\frac{\partial H}{\partial r} + k_\theta\frac{d\theta}{d\tau} + k_\varphi \sin\theta\frac{d\varphi}{d\tau} \quad (7)$$

$$\frac{dk_\theta}{d\tau} = \frac{1}{r}\left(-\frac{\partial H}{\partial \theta} - k_\theta\frac{dr}{d\tau} + k_\varphi r\cos\theta\frac{d\varphi}{d\tau}\right) \quad (8)$$

$$\frac{dk_\varphi}{d\tau} = \frac{1}{r\sin\theta}\left(-\frac{\partial H}{\partial \varphi} - k_\varphi\sin\theta\frac{dr}{d\tau} - k_\varphi r\cos\theta\frac{d\theta}{d\tau}\right) \quad (9)$$

Propagation vector elements in spherical polar coordinates r,Θ,φ	
f	The frequency of the electromagnetic signal
H	Hamiltonian
Kr, KΘ, and Kφ	
P'	P'=ct, group path
r,Θ,φ	Coordinates of Polar space that is spherical
π	π ≈3.14
ω	The frequency of angular waves, 2πf

The inputs are separated into two groups: first, the parameters that describe the ionosphere analysis models and the data that control the type of ray paths required, and second, the data that are required if non analytical ions are used. The following points can be used to summarize the output: printout, RT drawing, and punched card. Every time the ray passes the receiving device's height; a leap is computed. The program's beginning conditions are to ascertain the direction of transmission, the wave frequency, and the transit position; these conditions are prepared for each ray, the radiation tracing program was precise and adaptable.

(Zaalov et al., 2005)[58]**,** In this paper, simulations using John and Stevenson codes are used, to use an ionosphere model to calculate the ray trajectories from the transmitter site. A model has been developed so that the mechanics of propagation are completely comprehended and incorporated into pred iction systems. Some modifications were made to the Jones and Stevenson program, including time-varying parameters, modifications made to the homing procedure and changes in sizes of (azimuth and elevation step size) to improve execution speed. After these modifications, Ray tracing necessitates an ion osphere model where the profile of electron density and the refractive index gradient are continuous, so a modifiable model of the profile of electron density has been created.

(Bianchi et al., n.d.)[59] In this paper, the virtual and computed time delays of 3D ray tracing are compared, where the computed time delay is a number that enables the Ray Tracing's effectiveness pr ocedure to be examined under the assumption that the 3D ionosphere model is accurate and The delay in virtual time is presumed to be real-time. The comparison is made by simulating an ideal reflector placed at the virtual height, and the researchers found that the ray tracing algorithm's integration of differential e quations is the cause of the minuscule relative errors, which are consistently less than 0.2% and the numerical electron density profiles. The simulated reflector's consequent apparent height and the calculated apparent height were verified and when the region of interest in the ionosphere does not reach t he maximum electron density, the little discrepancies between the two measurements are always less than 1%.

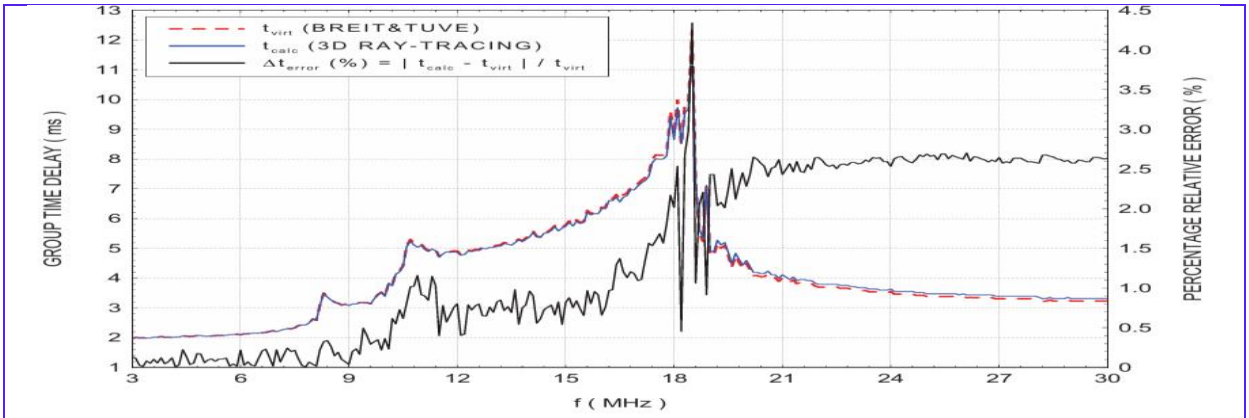

Figure 14 : Virtual time delay is represented by the red line, the estimated delay in time is shown by the blue line, th e proportional discrepancy between the computed and virtual delays is shown by the black line.

(Density, n.d.)[60] In this paper, The impact of horizontal ionosphere gradients in three dimens ions (altitude, longitude, and latitude) is taken into account when building an accurate numerical ray traci ng model. An electron density model in three dimensions is used for this where the ionosphere can be accurately modeled through fitting it to an IRI model over a wide latitude, longitude, and altitude range and including continuous spatial derivatives. The researchers conclude that the new subprogram enables 3D Jones GPS ray tracing through the atmosphere. In addition, the findings of the simulation are used to c alculate the residual range error (RRE).

(Erdem et al., 2015)[2] IONOLAB-RAY is a software module in this paper application designe d to stand in for the ray tracing in a wave propagation model based on ray tracing over a spherical 3D gri d model of the ionosphere and determining the refractive index utilizing the Appleton-Hartree formulas a nd the IRI-Plas-G model to determine the ionosphere's physical properties, Like any other wave, it splits i nto two pieces as it approaches the ionosphere and an exceptional wave, which is visible from the progra m outputs as depicted in figure (16).

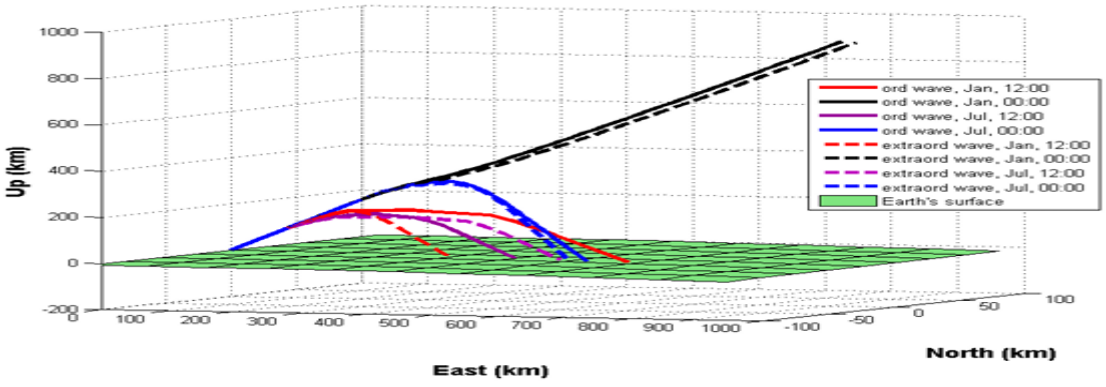

Figure 15: Discover both typical and exceptional waves, day or night, winter or summer.

(Warrington et al., 2016) [61], To simulate how high-frequency communications are affected by the polar ionosphere and to determine the locations of the total electronic content, a signal-tracking technique was used with the main ionospheric parameters derived from the IRI model. This study is important for improving the techniques of instantaneous forecasting and prediction of the propagation of waves at high frequencies at polar latitudes.

(Fagre et al., 2020)[6]**,** This work offers an altered form of the traditional 3D numerical ray tracing code, connected to models of mobile ionospheric disturbances (TIDs), the Earth's mag netic field, the neutral atmosphere and the ionosphere. This technique mimics wave propagation i n the turbulent ionosphere to investigate how TIDs affect radio waves. To address discontinuities and guarantee the validity and precision of the ray tracing in all circumstances, the ray tracing a lgorithm uses the 3D cubic interpolation method. The ionosphere acts as a reflector for high-freq uency (HF) radio signals, extending their ground range. Since electromagnetic waves propagate th rough the ionosphere in a theoretically complex manner, Ray tracing is frequently employed to re solve this issue since it enables us to determine the precise trajectory of radio waves. The curren t study examines how medium-range TIDs (MSTIDs) affect a few HF beam path parameters. Ray path modifications are obtained by TID simulations using Jones and Stevenson's 3D ray tracing technique. The approach based on the algorithm developed by Jones and Stevenson allows to choose of any ionospheric background settings and TID properties in an actual geomagnetic field. Th e ray tracing code that has been implemented is capable of implementing every mode of propagati on: HF signal ray tracing model, TID model, and interpolation and integration method. Results: Th e transmitted radio waves' azimuth angle varied between 60° and 120° in two ionospheric scenar ios, with a 5° step: circumstances that are not disturbed and with overlapping TID. As the freque ncy increases, the ground range and reflection heights of the waves reflected from the designated layers (white tracks) rise until they reach the Pedersen beam (black tracks). This work's objective is to offer a ray tracing method that functions under variable and near to actual conditions, and the beam would bend away from the minimum frequency rise in the case of the maximum usef ul frequency.

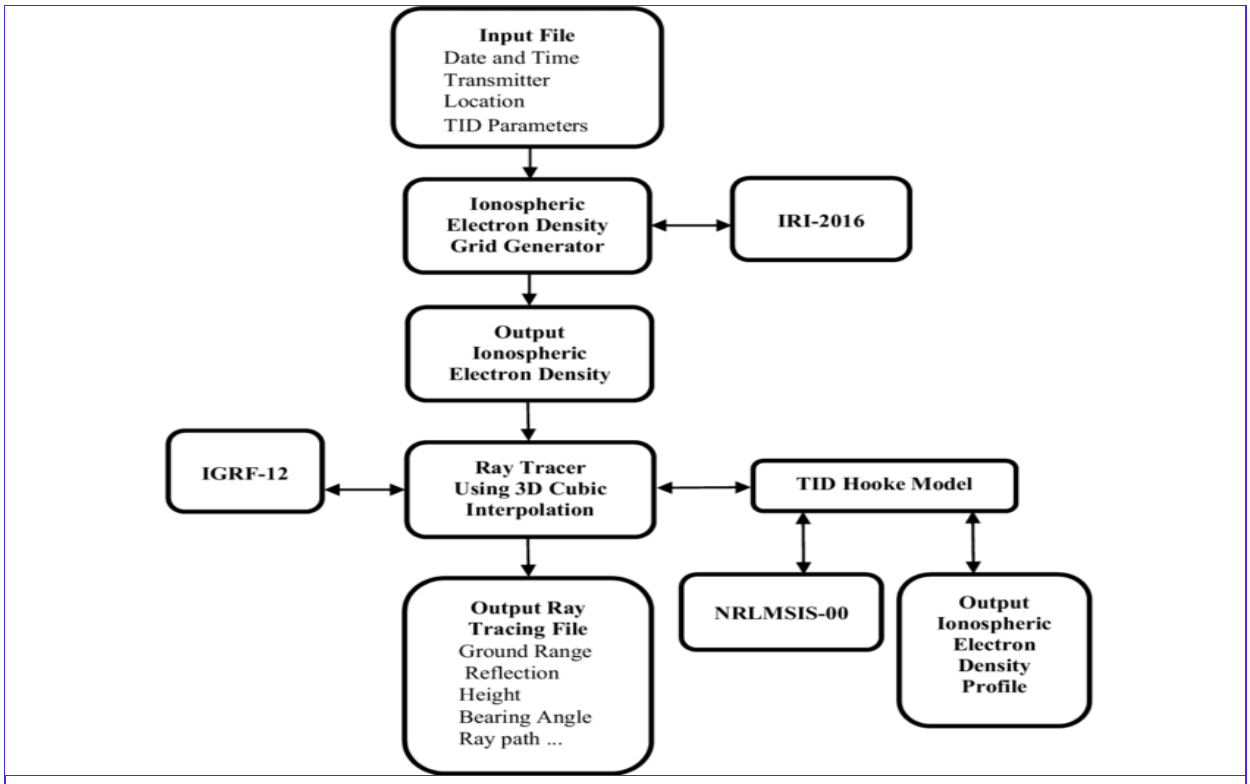

Figure 16: Code flowchart for ray Tracing according to Stephenson and Jones, altered to provide linkages to many models and a cubic interpolation technique.

(Pietrella et al., 2023)[11] In this paper, the researchers rewrote the code for the Jones and Stevenson report from Fortran 77 to Fortran 90, relying on The IRI model's electron density background to improve the IONORT (IONOSPHER RAY TRACING) programming tool that is utilized to ascertain t he trajectory of high-frequency waves from propagation in the middle of the ionosphere, one of the major modifications is the substitution of a global electron density matrix in three dimensions for the regional one that was previously used as input to depict the ionosphere. Thus, the latest graphical user interface (G UI) for ray tracing makes it feasible to do various ray tracings from any location on the surface of the Ear th by just choosing appropriate loop cycles. the scope of this tool was expanded from the regional level to the global scale where users can perform their simulations anywhere and the possibility of conducting homing simulation and get the three outputs (frequency, elevation angle, and azimuth angle).

(Jiang, Lei, and Yue 2024)[62]In this paper, the authors proposed a novel approach for deriving the electron density profile from ionograms using a Ray Tracing Inversion Method (RTIM). The aim of the study is to enhance the accuracy of ionospheric modeling by retrieving a more realistic electron density profile compared to conventional techniques. The methodology involves starting with an initial guess of the electron density model and then applying a ray tracing algorithm to simulate the radio wave propagation through the ionosphere. The resulting simulated ionogram is then compared with the observed ionogram, and the model is iteratively adjusted until both match closely. The results demonstrate that the proposed method significantly improves the accuracy of the retrieved electron density profile, particularly in the upper F-region. The simulated ionograms closely resemble the observed data, indicating the effectiveness of the inversion process. The study concludes that RTIM is a powerful tool for refining electron density profiles from ionospheric observations and can contribute to better performance in radio communication systems that rely on ionospheric propagation.

(Molina et al., 2024)[63]**,** Ray tracing simulated was developed, designed, and tested based on the Jones and Stevenson report (1975) written in Fortran 77 that is difficult to maintain, so an accurate and well-working program has been developed at frequencies above 2 MHZ using a bubble model. New 3D equatorial plasma along with ionosphere, atmosphere, and magnetic heterogeneous plasma. The simulation structure and algorithms used to solve the ray tracing equation were preserved, as the simulation was performed by randomly changing the discharge around the zenith. The results of the simulation were as shown in figure 18, There was not much of a discrepancy between the modified model and the original m odel.

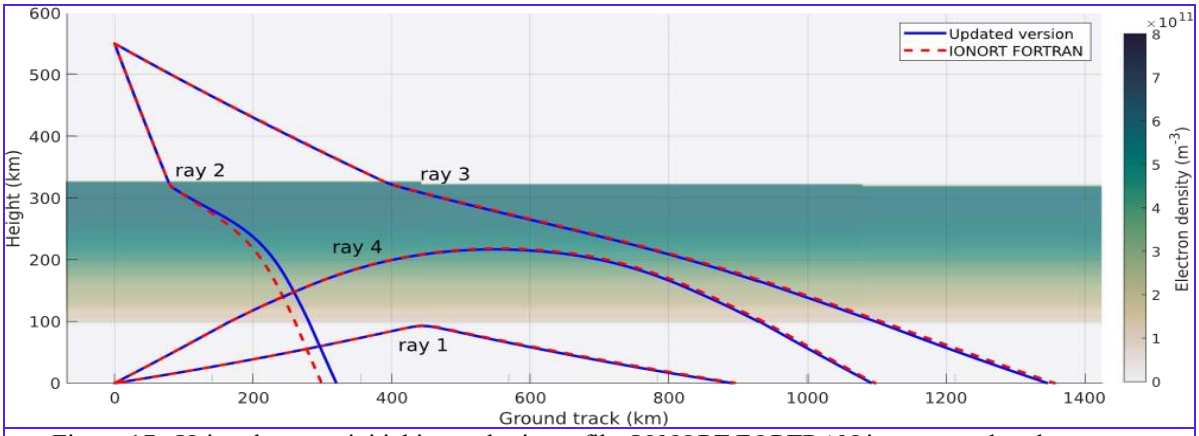

Figure 17 : Using the same initial ionospheric profile, IONORT FORTRAN is compared to the current software. Blue lines indicate the output of the four ray simulations using the default settings in the current software, while red lines show the older version in FORTRAN.

The combination of MATLAB with FORTRAN necessitates the usage of text files for variables and outcomes of input/output, which complicates the programs and slows down calculation.

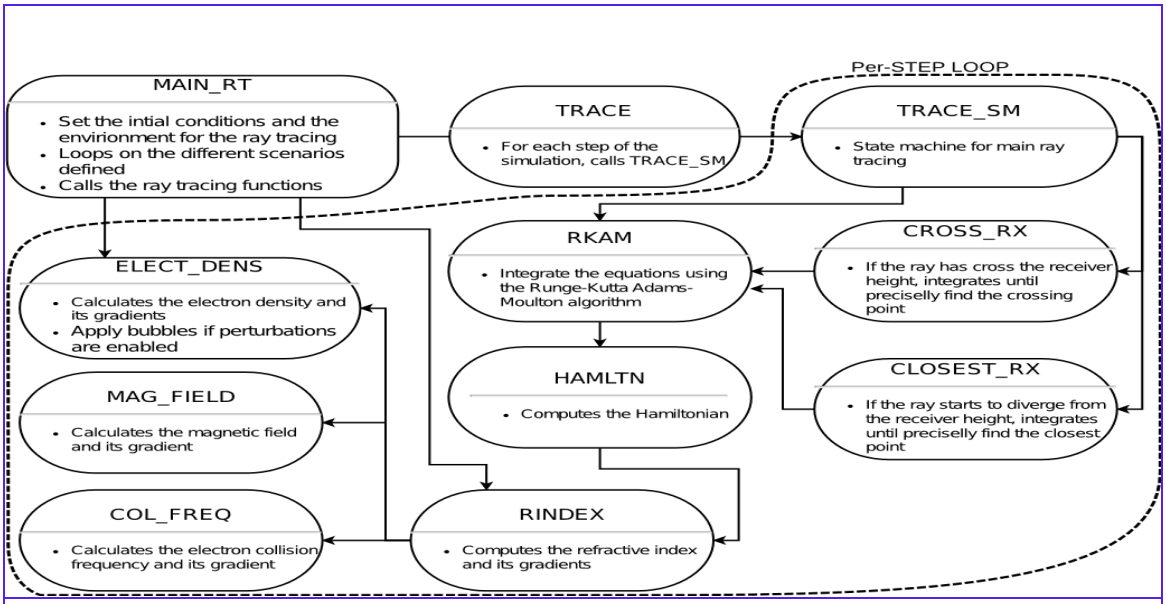

Figure 18: The software block diagram for tracking ionospheric rays and an overview of its features, Arrows show function calls.

Numerous scholars examined the Jones and Stevenson study and made modifications and enhancements

to reflect recent advancements. One software program has added FORTRAN as a subroutine to the MATLAB GUI, making it easier to enter variables and display the outcomes visually. The software, which goes by the name IONORT, has been released multiple times in the last few years. This method's disadvantage is that only minor changes to the models employed are possible because the underlying code is still written in FORTRAN.

5 Conclusion

Before the discovery of the ionosphere, electronic communications could not be made over a distance of more than 100 km because of the Earth's curvature, however upon its discovery, electronic communications could be made over a distance of more than 3000 km thanks to Radio waves' passage thr ough the ionosphere. The ionosphere has no electrical charge, its height varies between 50 and 1000 km, and depending on geomagnetic activity, its outer limit may surpass 3000 km.

High frequency communications allow signals to propagate through the ionosphere, the propagation of high-frequency signals depends on the electron density, it is important to obtain reliable electron density and frequency values for transmissions in ionospheric wave propagation. This paper is A summary of the ionosphere, The consequences of solar activity, and geomagnetic storms on the ionosphere. The most sig nificant empirical model responsible for describing the ionospheric parameters, one popular standard for c haracterizing ionosphere properties is the International Reference Ionosphere (IRI), that decreases the eff ects of high-frequency waves by using the ray tracing approach to forecast monthly average Ion temperat ure, ion composition, electron temperature, and electron density, Through a variety of processes, includin g attenuation, refraction, reflection, absorption, and scattering, the ionospheric effects weaken the signal. Therefore, the impacts on the propagation of high-frequency radio waves through the ionosphere were de termined by analyzing and summarizing a number of researches on the topic of ray tracing using data from the IRI ionosphere model.

In future research, we'll work to enhance high-frequency waves' ability to travel across the ionosp here and minimize their impact by using a new model for ray tracing technology and relying on the information from the IRI model.

Author Contributions: The authors contributed to all parts of the current study.
Funding: This study received no external funding.
Conflicts of Interest: The authors declare no conflict of interest.

Reference

[1] H. Abbas and H. Al-Behadili, "Propagation Model for Nowcasting of HF Communications with Aircraft on Polar Routes," no. March, 2018.
[2] E. Erdem, F. Ankan, M. N. Deviren, and I. Cor, "A model based ray tracing algorithm for anisotropic and inhomogeneous ionosphere with GIM-TEC assimilation," *RAST 2015 - Proc. 7th Int. Conf. Recent Adv. Sp. Technol.*, pp. 477–481, 2015, doi: 10.1109/RAST.2015.7208392.
[3] M. Atiq, "Historical review of ionosphere in perspective of sources of ionization and radio waves propagation," *Res. Rev. J. Sp. Sci. Technol.*, vol. 7, no. 2, pp. 28–39, 2018.
[4] D. Bilitza, "IRI the international standard for the ionosphere," *Adv. Radio Sci.*, vol. 16, pp. 1–11, 2018, doi: 10.5194/ars-16-1-2018.
[5] T. G. Cameron, R. A. D. Fiori, E. M. Warrington, A. J. Stocker, T. Thayaparan, and D. W. Danskin, "Characterization of high latitude radio wave propagation over Canada," *J. Atmos. Solar-Terrestrial Phys.*, vol. 219, pp. 1–19, 2021, doi: 10.1016/j.jastp.2021.105666.
[6] M. Fagre, B. S. Zossi, J. Chum, and A. G. Elias, "Simulated high frequency ray paths considering

traveling ionospheric disturbances," *SN Appl. Sci.*, vol. 2, no. 4, pp. 1–8, 2020, doi: 10.1007/s42452-020-2438-4.

[7] K. Davies, *Ionospheric Radio*. 1990. doi: 10.1049/pbew031e.

[8] M. Hervás, P. Bergadà, and R. M. Alsina-Pagès, "Ionospheric narrowband and wideband HF soundings for communications purposes: A review," *Sensors (Switzerland)*, vol. 20, no. 9, 2020, doi: 10.3390/s20092486.

[9] S. B. Ganguli, "Ionospheres physics, plasma physics and chemistry," *J. Atmos. Solar-Terrestrial Phys.*, vol. 65, no. 6, p. 779, 2003, doi: 10.1016/s1364-6826(03)00002-6.

[10] D. Bilitza, M. Pezzopane, V. Truhlik, D. Altadill, B. W. Reinisch, and A. Pignalberi, "The International Reference Ionosphere Model: A Review and Description of an Ionospheric Benchmark," *Rev. Geophys.*, vol. 60, no. 4, 2022, doi: 10.1029/2022RG000792.

[11] M. Pietrella, M. Pezzopane, A. Pignatelli, A. Pignalberi, and A. Settimi, "An Updating of the IONORT Tool to Perform a High-Frequency Ionospheric Ray Tracing," *Remote Sens.*, vol. 15, no. 21, 2023, doi: 10.3390/rs15215111.

[12] A. Komjathy, "Global Ionospheric Total Electron Content Mapping Using the Global Positioning System," *Engineering*, no. 188, p. 248, 1997, [Online]. Available: http://www2.unb.ca/gge/Pubs/TR188.pdf

[13] V. Bidula, "Dynamic Model of the Ionosphere for Wide-Field Radio Experiments," 2023.

[14] Y. Liu *et al.*, "Review of ionospheric irregularities and ionospheric electrodynamic coupling in the middle latitude region," *Earth Planet. Phys.*, vol. 5, no. 5, pp. 462–482, 2021, doi: 10.26464/epp2021025.

[15] J. M. Grebowsky and A. C. Aikin, "Planetary ionospheres - Sources and dynamic drivers," *Proc. Int. Astron. Union*, vol. 4, no. 257, pp. 499–510, 2008, doi: 10.1017/S1743921309029780.

[16] L. B. Liu, W. X. Wan, Y. D. Chen, and H. J. Le, "Solar activity effects of the ionosphere: A brief review," *Chinese Sci. Bull.*, vol. 56, no. 12, pp. 1202–1211, 2011, doi: 10.1007/s11434-010-4226-9.

[17] R. S. Dabas, K. Sharma, R. M. Das, N. K. Sethi, K. G. M. Pillai, and A. K. Mishra, "Ionospheric modeling for short- And long-term predictions of F region parameters over Indian zone," *J. Geophys. Res. Sp. Phys.*, vol. 113, no. 3, 2008, doi: 10.1029/2007JA012539.

[18] A. A. Al-Shallal and N. M. R. Al-Ubaidi, "Comparing ionospheric MUF using IRI16 model with mid-latitude ionosonde observations and associated with strong geomagnetic storms," *Iraqi J. Sci.*, vol. 61, no. 12, pp. 3434–3445, 2020, doi: 10.24996/ijs.2020.61.12.31.

[19] D. Buresova, "Effects of geomagnetic storms on the bottomside ionospheric F region," *Adv. Sp. Res.*, vol. 35, no. 3, pp. 429–439, 2005, doi: 10.1016/j.asr.2005.03.032.

[20] T. J. Fuller-Rowell, M. V. Codrescu, R. J. Moffett, and S. Quegan, "Response of the thermosphere and ionosphere to geomagnetic storms," *J. Geophys. Res. Sp. Phys.*, vol. 99, no. 3, pp. 3893–3914, 1994, doi: 10.1029/93JA02015.

[21] D. V. Blagoveshchenskii, "Effect of geomagnetic storms (substorms) on the ionosphere: 1. A review," *Geomagn. Aeron.*, vol. 53, no. 3, pp. 275–290, 2013, doi: 10.1134/S0016793213030031.

[22] D. Buresova, J. Lastovicka, and G. De Franceschi, "Manifestation of Strong Geomagnetic Storms in the Ionosphere above Europe," pp. 185–202, 2007, doi: 10.1007/1-4020-5446-7_17.

[23] D. Vijaya Lekshmi, N. Balan, S. Tulasi Ram, and J. Y. Liu, "Statistics of geomagnetic storms and ionospheric storms at low and mid latitudes in two solar cycles," *J. Geophys. Res. Sp. Phys.*, vol. 116, no. 11, pp. 1–13, 2011, doi: 10.1029/2011JA017042.

[24] V. A. Ivanov, N. V. Ryabova, R. R. Belgibaev, and A. A. Chernov, "Efficiency of HF Communication Modems Operating over a Mid-latitude Long-Range Propagation Path," *2018 Syst. Signal Synchronization, Gener. Process. Telecommun. SYNCHROINFO 2018*, no. 2, pp. 1–5, 2018, doi: 10.1109/SYNCHROINFO.2018.8457021.

[25] M. J. Conway, C. J. Payne, S. G. Bilén, and E. N. Koski, "Ground-wave propagation characterization and prediction for HF cognitive radio," *Proc. - IEEE Mil. Commun. Conf. MILCOM*, vol. 2015-Decem, pp. 1643–1649, 2015, doi: 10.1109/MILCOM.2015.7357680.

[26] H. Rishbeth, "Ionospheric dynamics 1945-1970," *J. Atmos. Terr. Phys.*, vol. 36, no. 12, pp. 2309–

2319, 1974, doi: 10.1016/0021-9169(74)90153-6.
[27] R. Communication and V. I. A. Near, "MASTER ' S THESIS RADIO COMMUNICATION VIA NEAR," no. May, 2021.
[28] D. Bilitza, K. Rawer, L. Bossy, and T. Gulyaeva, "International reference ionosphere - past, present, and future: II. Plasma temperatures, ion composition and ion drift," *Adv. Sp. Res.*, vol. 13, no. 3, pp. 15–23, 1993, doi: 10.1016/0273-1177(93)90241-3.
[29] D. Bilitza, "International Reference Ionosphere 2000 of ionospheric It was and the F peak down to," *Radio Sci.*, vol. 36, no. 2, pp. 261–275, 2001.
[30] D. Bilitza, L. A. McKinnell, B. Reinisch, and T. Fuller-Rowell, "The international reference ionosphere today and in the future," *J. Geod.*, vol. 85, no. 12, pp. 909–920, 2011, doi: 10.1007/s00190-010-0427-x.
[31] D. Bilitza and B. W. Reinisch, "International Reference Ionosphere 2007: Improvements and new parameters," *Adv. Sp. Res.*, vol. 42, no. 4, pp. 599–609, Aug. 2008, doi: 10.1016/j.asr.2007.07.048.
[32] K. Rawer, D. Bilitza, and S. Ramakrishnan, "Goals and status of the International Reference Ionosphere," *Rev. Geophys.*, vol. 16, no. 2, pp. 177–181, 1978, doi: 10.1029/RG016i002p00177.
[33] D. Bilitza *et al.*, "The International Reference Ionosphere 2012 - A model of international collaboration," *J. Sp. Weather Sp. Clim.*, vol. 4, 2014, doi: 10.1051/swsc/2014004.
[34] D. Bilitza, D. Altadill, V. Truhlik, M. Friedrich, and V. Shubin, "International Reference Ionosphere -Update 2020," no. September, p. 34158, 2021, doi: 10.1029/2018JA025437.
[35] M. Yasar, S. Sagir, L. Y. Emelyanov, M. V. Lyashenko, S. Korlaelci, and R. Atici, "Calculation of the Ionospheric Cross-Section with the Incoherent Scattering Radar and Its Comparison with the Predictions of the IRI Model," *Wirel. Pers. Commun.*, vol. 132, no. 1, pp. 487–503, 2023, doi: 10.1007/s11277-023-10619-6.
[36] D. Bilitza, S. Bhardwaj, and C. Koblinsky, "Improved IRI predictions for the GEOSAT time period," *Adv. Sp. Res.*, vol. 20, no. 9, pp. 1755–1760, 1997, doi: 10.1016/S0273-1177(97)00585-1.
[37] A. Komjathy, R. B. Langley, and D. Bilitza, "Ingesting GPS-derived TEC data into the international reference ionosphere for single frequency radar altimeter ionospheric delay corrections," *Adv. Sp. Res.*, vol. 22, no. 6, pp. 793–801, 1998, doi: 10.1016/S0273-1177(98)00100-8.
[38] B. Nava, S. M. Radicella, and F. Azpilicueta, "Data ingestion into NeQuick 2," vol. 46, no. June, pp. 1–8, 2011, doi: 10.1029/2010RS004635.
[39] D. Bilitza *et al.*, "International Reference Ionosphere 2016: From ionospheric climate to real-time weather predictions," *Sp. Weather*, vol. 15, no. 2, pp. 418–429, 2017, doi: 10.1002/2016SW001593.
[40] M. Hernandez-Pajares, J. M. Juan, J. Sanz, and D. Bilitza, "Combining GPS measurements and IRI model values for space weather specification," *Adv. Sp. Res.*, vol. 29, no. 6, pp. 949–958, 2002, doi: 10.1016/S0273-1177(02)00051-0.
[41] N. Ssessanga, Y. H. Kim, E. Kim, and J. Kim, "Regional optimization of the IRI-2012 output (TEC, foF2) by using derived GPS-TEC," *J. Korean Phys. Soc.*, vol. 66, no. 10, pp. 1599–1610, 2015, doi: 10.3938/jkps.66.1599.
[42] J. B. Habarulema and N. Ssessanga, "Adapting a climatology model to improve estimation of ionosphere parameters and subsequent validation with radio occultation and ionosonde data," *Sp. Weather*, vol. 15, no. 1, pp. 84–98, 2017, doi: 10.1002/2016SW001549.
[43] A. Pignalberi, J. B. Habarulema, M. Pezzopane, and R. Rizzi, *On the Development of a Method for Updating an Empirical Climatological Ionospheric Model by Means of Assimilated vTEC Measurements From a GNSS Receiver Network*, vol. 17, no. 7. 2019. doi: 10.1029/2019SW002185.
[44] A. Pignalberi, M. Pietrella, and M. Pezzopane, "Towards a real-time description of the ionosphere: A comparison between international reference ionosphere (iri) and iri real-time assimilative mapping (irtam) models," *Atmosphere (Basel).*, vol. 12, no. 8, 2021, doi: 10.3390/atmos12081003.
[45] I. A. Galkin, B. W. Reinisch, X. Huang, and D. Bilitza, "Assimilation of GIRO data into a real-time IRI," vol. 47, no. April, pp. 1–10, 2012, doi: 10.1029/2011RS004952.
[46] E. Timoçin, I. Ünal, and D. Göker, "A Comparison of IRI-2016 foF2 Predictions with the Observations at Different Latitudes During Geomagnetic Storms," *Geomagn. Aeron.*, vol. 58, no. 7, pp. 846–856, 2018, doi: 10.1134/S0016793218070216.

[47] M. Fagre, B. S. Zossi, J. Chum, E. Yiğit, and A. G. Elias, "Ionospheric high frequency wave propagation using different IRI hmF2 and foF2 models," *J. Atmos. Solar-Terrestrial Phys.*, p. 105141, 2019, doi: 10.1016/j.jastp.2019.105141.

[48] J. Kim and Y. Kwak, "ScienceDirect Validating the IRI-2020 model for ionospheric storms over the North-East Asian sector induced by extreme geomagnetic storms," *Adv. Sp. Res.*, no. xxxx, 2024, doi: 10.1016/j.asr.2024.07.032.

[49] E. D. Height, "A New Determining Method for Ionospheric F2-Region Peak Electron Density Height," 2024.

[50] A. Ubaidi, N. M. R. Al Ubaidi, R. Falih, H. Foadi, and S. I. Gburi, "Disturbances of Ionospheric Total Electron Content during Great and Severe Geomagnetic Storms above Iraq and Surrounding Areas" vol. 65, no. 10, pp. 6134–6153, 2024, doi: 10.24996/ijs.2024.65.10(SI).20.

[51] H. Hazim and N. M. R. Al-ubaidi, "Investigating the Effect of Sudden Stratospheric Warming on the Ionosphere above Basrah City," vol. 23, no. 1, pp. 122–137, 2025.

[52] E. B. Seba and S. Poedts, "ScienceDirect Assessment of IRI2020 model accuracy in predicting ionospheric parameters : Insights from multiple ionosonde stations," *Adv. Sp. Res.*, vol. 75, no. 1, pp. 918–935, 2025, doi: 10.1016/j.asr.2024.09.026.

[53] L. C. Tsai, C. H. Liu, and J. Y. Huang, "Three-dimensional numerical ray tracing on a phenomenological ionospheric model," *Radio Sci.*, vol. 45, no. 5, pp. 1–11, 2010, doi: 10.1029/2010RS004359.

[54] Z. Yun and M. F. Iskander, "Ray tracing for radio propagation modeling: Principles and applications," *IEEE Access*, vol. 3, pp. 1089–1100, 2015, doi: 10.1109/ACCESS.2015.2453991.

[55] L. Vandergriff, "Nature and Properties of Light," *Fundam. Photonics*, no. June, pp. 1–38, 2009, doi: 10.1117/3.784938.ch1.

[56] C. Darwin, "This is a reproduction of a library book that was digitized by Google as part of an ongoing effort to preserve the information in books and make it universally accessible. https://books.google.com," *Oxford Univ.*, vol. XXX, p. 60, 1895.

[57] S. C. Aune, "Comparison of Ray Tracing through Ionospheric Models," 2006.

[58] N. Y. Zaalov, E. M. Warrington, and A. J. Stocker, "A ray-tracing model to account for off-great circle HF propagation over northerly paths," *Radio Sci.*, vol. 40, no. 4, pp. 1–14, 2005, doi: 10.1029/2004RS003183.

[59] C. Bianchi, A. Settimi, C. Scotto, A. Azzarone, and A. Lozito, "A method to test HF ray tracing algorithm in the ionosphere by means of the virtual time delay," pp. 1–17.

[60] A. V. E. Density, "Ray Tracing in Realistic 3D Ionospheric Model," pp. 267–272.

[61] E. M. Warrington *et al.*, "Near real-time input to a propagation model for nowcasting of HF communications with aircraft on polar routes," *Radio Sci.*, vol. 51, no. 7, pp. 1048–1059, 2016, doi: 10.1002/2015RS005880.

[62] Q. Jiang, J. Lei, and X. Yue, "Electron Density Profile Derived From Ionogram Using Ray Tracing Inversion Method Electron Density Profile Derived From Ionogram Using Ray," no. December, 2024, doi: 10.1029/2024RS008086.

[63] C. Molina, E. Fernandez-Nion, and A. Camps, "Modern Ionospheric Ray Tracer for Earth Observation Satellite Missions," *IEEE J. Sel. Top. Appl. Earth Obs. Remote Sens.*, vol. 17, pp. 13244–13260, 2024, doi: 10.1109/JSTARS.2024.3421509.